Accepted Manuscript

The contact drag of towed demersal fishing gear components

F.G. O'Neill, K.J. Summerbell, A. Ivanović

PII: S0924-7963(17)30200-2
DOI: doi: 10.1016/j.jmarsys.2017.08.002
Reference: MARSYS 3006

To appear in: *Journal of Marine Systems*

Received date: 3 May 2017
Revised date: 18 August 2017
Accepted date: 28 August 2017

Please cite this article as: F.G. O'Neill, K.J. Summerbell, A. Ivanović , The contact drag of towed demersal fishing gear components, *Journal of Marine Systems* (2017), doi: 10.1016/j.jmarsys.2017.08.002

the contact drag of towed demersal fishing gear components.

F. G. O'Neill[1*], K.J. Summerbell and A. Ivanović[2]

[1]Marine Scotland Science, Marine Laboratory,

375 Victoria Road, Aberdeen, AB11 9DB, Scotland.

[2]University of Aberdeen, School of Engineering,

Kings College, Aberdeen, AB24 3UE, Scotland.

[*]Corresponding author.

b.oneill@marlab.ac.uk

Abstract

The contact demersal towed fishing gears make with the seabed can lead to penetration of the substrate, lateral displacement of the sediment and a pressure field transmitted through the sediment. It will also contribute to the overall drag of the fishing gear. Consequently, there can be environmental effects such as habitat alteration and benthic mortality, and impacts to the fuel efficiency of the fishing operation which will affect emissions of nitrogen oxides, sulphur oxides and greenhouse gases such as CO2. Here we present the results of experimental trials that measure the contact drag of a range of elements that represent some of the components of towed demersal gears that are in contact with the seabed.

We show that the contact drag of the gear components depends on their weight, geometry, the type of sediment on which they are towed and whether they are rolling or not. As expected, the contact drag of each gear component increases as its weight increases and the drag of fixed elements is greater than that of the rolling ones. The dependence on aspect ratio is more complex and the drag (per unit area) of narrow cylinders is less than that of wider ones when they roll on the finer sediment or are fixed (not permitted to roll) on the coarser sediment. When they roll on the coarse sediment there is no dependence on aspect ratio. Our results also suggest that fixed components may penetrate the seabed to a lesser depth when they are towed at higher speeds but when they roll there is no such relationship.

keywords: trawl fishing gears; environmental impact of fishing; contact drag; benthic impact of fishing

highlights:

we measure the contact drag of a range of fishing gear components

the contact drag depends on the weight and geometry of a component

the contact drag depends on sediment type and whether the components roll or are fixed

the contact drag of rolling components does not seem to be dependent on towing speed

1 Introduction

Mobile bottom-contacting fishing gears, which capture fish and crustacean species that live close to or on the seabed, account for about 23% of global fisheries yield (FAO, 2009). As they are dragged or towed across the seabed these gear have physical impacts on the benthic environment which have been classified as being either geotechnical or hydrodynamic (O'Neill and Ivanović, 2016; O'Neill and Summerbell, 2011). The geotechnical effects refer to the contact drag, the penetration and piercing of the substrate, lateral displacement of sediment and the influence of the pressure field transmitted through the sediment; whereas the hydrodynamic effects refer to the hydrodynamic drag and the mobilisation of sediment into the water column.

Eigaard et al. (2016) categorise the most common mobile bottom-contacting fishing gears as being otter trawls, demersal seines, beam trawls or dredges (Figure 1). They are made of a range of components, some of which, such as otter doors, sweeps, seine ropes, beam trawl shoes, groundgear, tickler chains, dredge teeth etc., physically impact the seabed (Figures 1 and 2). Many studies have shown that these impacts can damage habitats, cause benthic mortality, release nutrients and resuspend phytoplankton cysts and copepod eggs (Kaiser et al., 2006; Dounas et al., 2007; Gilkinson et al., 1998; Brown et al., 2013; Drillet et al., 2014; O'Neill et al., 2013a; Oberle et al., 2016). Hence, in order to manage fisheries in a sustainable manner and develop more environmentally friendly fishing techniques, we must understand the underpinning hydrodynamic and geotechnical processes associated with towing these gear components across the seabed.

O'Neill and Summerbell (2016) examine the hydrodynamic effects of these components and here we focus on the geotechnical effects and investigate the contact drag of cylindrical and rectangular shaped objects that are in contact with the seabed.

There have been many observations of the alteration of the seabed following the passage of towed fishing gears using both acoustic methods (Lucchetti and Sala, 2012; O'Neill *et al*., 2013b; Palanques *et al*., 2014; Humborstad *et al*., 2014; Depestele *et al*., 2016) and optical methods (O'Neill *et al*., 2009; Puig *et al*., 2012; Boulcott *et al*., 2014).

More focused geotechnical studies have taken place under laboratory conditions in sand channels and have concentrated on developing a better understanding of the fundamental processes and developing small scale modeling rules so results from channel experiments can be transferred to the full scale (Paschen *et al*., 2002; Enerhaug *et al*., 2012, Ivanović and Casanovas Revilla, 2013; Esmaeili and Ivanović, 2014). Numerical models of the geotechnical interaction of fishing gears with the seabed have also been developed, the more recent of which predict the contact forces and penetration into the seabed of individual gear components (Ivanović *et al*., 2011; Ivanović and O'Neill, 2015; Esmaeili and Ivanović, 2014). While these studies have all contributed to our understanding of the interaction of fishing gears on the benthic environment, they are often gear and sediment specific. There is a need to generalise results and improve our capacity to predict impacts of different gear components on a range of sediment types.

Here, we address some of these issues by making quantitative full-scale measurements of the geotechnical impacts of well-defined gear components on the seabed. We examine a range of rigid cylindrical and rectangular shaped objects and examine how their contact drag varies with speed, weight, geometry (aspect ratio), sediment type and for the cylindrical components, whether they are rolling or are fixed.

2 Materials and Methods

2.1 Towed sledge and instrumentation

Experimental sea trials were carried out on the RV Alba na Mara during October 2013 and May 2015 in the inner Moray Firth, Scotland using the same towed sledge as O'Neill and Summerbell (2016). The sledge was 0.9m high, 2.1m wide, 3.0m long and weighed 530kg and towed 14 different types of cylindrical, disk and rectangular elements supported on an axle that is 1.3m long and 63mm in diameter (Figure 3). The full range of these elements is presented in Figure 4, the dimensions of which are presented in Table 1. The elements were chosen to simulate a range of gear components that are in contact with the seabed (roller clumps, groundgears, otter doors, etc) (Figure 2). The cylindrical and disk elements span the aspect ratio categories of Godwin and O'Dogherty (2007) who classify the aspect ratio of their objects as being wide ($d/b < 0.5$), narrow ($1 < d/b < 6$) and very narrow ($d/b > 6$) where d and b are the diameter and breadth of the cylinder/disk respectively (Table 1). In addition, we classify objects in the range $0.5 < d/b < 1$ as being intermediate.

Strainstall 500kg *X*-*Y* load cells were fitted at each end of the axle to measure the force in the horizontal plane at a rate of 10Hz, where the *X*-axis is along the axle and the *Y*-axis in along the towing direction. This force comprises the hydrodynamic drag forces acting on the gear component and on the supporting axle as they are towed through the water and the contact drag force acting on the component as it is pulled across the seabed. Hence the contact drag is estimated by subtracting the hydrodynamic drags from the forces measured by the load cells.

The axle was attached to a framework (via the load cells) that was free to move in the vertical direction (Figure 5). Thus, the vertical forces that the gear elements exerted on the sea bed were the gravitational forces associated with the gear element and that part of the supporting

framework that was free to move. It was also possible to increase the applied vertical forces by attaching weights to the framework and each of the configurations was tested having total vertical forces (in water) of approximately 588, 1176 and 1764 N. The speed at which the sledge was towed was increased incrementally over a thirty minute period during each deployment from 1 to 2 m/s. The vessels GPS recorded the speed of the sledge over the ground at a rate of 1Hz. The drag and speed data were time-averaged into 10s intervals and it is these data that are examined in the following analyses.

The 2013 trials took place on a sandy sediment in the Dornach Firth where all fourteen gear elements were examined: eight different cylinder designs; three configurations of separated disks; and three of rectangular doors (Figure 4). The cylindrical and disk designs were tested both when they were free to roll and when they were fixed. The 2015 trials took place approximately 8 miles north east of Tarbat Ness on a finer sediment where eight elements were tested: six of the cylindrical and two of the separated disk designs, all of which were free to roll.

To classify the sediment on which the trials took place, 15 grab samples were taken with a modified Day grab and the top 2.5 cm sampled and frozen, at each of the experimental sites. Subsequently these were defrosted and dried and the particle size distribution of each sample was analysed using a Malvern Instruments Mastersizer E Particle Size Analyser. An average was then taken to characterise the particle size distribution at each site.

2.2 Data analysis

The hydrodynamic drag of the gear components were calculated using the results of O'Neill and Summerbell (2016) who assume an expression of the following form

$$D = 0.5\rho A_{elem} U^2 c_d + 0.5\rho A_{axle} U^2 c_{axle}$$

where A_{axle} is the exposed frontal area of the axle, c_{axle} is its hydrodynamic drag coefficient, A_{elem} is the frontal area of the gear element and c_d represents c_{cyl}, c_{disk} or c_{door}, the hydrodynamic drag coefficients of the cylinders, the circular disks and the rectangular doors respectively. A_{axle} is calculated by multiplying the axle diameter by that part of the axle exposed to the oncoming flow and A_{elem} by multiplying the corresponding frontal dimensions of the gear elements (Figure 4 and Table 1). O'Neill and Summerbell (2016) show that when $c_{cyl} = c_{disk} = 0.64$, $c_{door} = 1.13$ and $c_{axle} = 0.93$, the above expression is a good fit to the hydrodynamic drag measurements they make for the gear elements used here. In order to compare results between gear elements, we standardise the resulting contact drag estimates and weight forces in relation to the area on which they act. We assume that for the cylinders the contact area scale is *bd* and for the elements with six disks it is 6*bd*. For the rectangular doors it is *bt*, where *b* is the breadth or width of the door, *t* is the door thickness and *h* is the vertical height (Table 1). Figure 6 contains the hydrodynamic drag per unit area estimates of O'Neill and Summerbell (2016) where the estimates are scaled per unit contact area which allows direct comparison with the scaled contract drag estimates.

We investigate the dependence of the contact drag forces on towing speed by fitting linear regressions to the data collected for each gear component for a given weight. We also explore the relationship between the contact drag per unit area and weight per unit area. Hambleton and Drescher (2009) have shown that for cylinders on the cohesive sediments there was a dependency on their aspect ratio (*d/b*), hence for this analysis we segregate the data accordingly and regress quadratic curves to the contact drag per unit area for each *d/b* value data set.

3 Results

The analysis of the Day grab sediment samples found the sediment at the 2013 site to have a silt and clay component (% of sediment < 63 μm) of 12% and a d_{50} of 100 μm. The sediment at the 2015 site was finer and had a silt and clay component of 30% and a d_{50} of 85 μm (Figure 7). The tidal currents were estimated to be on average 0.08 m/s, the average wind speed was 6 m/s and the sea state was generally slight to moderate.

As would be expected, the contact drag of each gear component increases as its weight increases. For the rectangular doors, the contact drag decreases as towing speed increases on the coarser sediment (Figure 8) and there appears to be a similar (albeit less clear-cut) tendency for the fixed disks and cylinders (Figure 9). However, for the rolling cylinders and disks there does not seem to be any consistent trend on either sediment (Figures 10 and 11).

The nature of the relationship between contact drag and component weight is more clearly expressed in Figures 12 – 15 which plot the same data as in Figures 8 - 11 but, this time, in terms of weight per unit area. These figures group together gear components with the same d/b value and demonstrate that the contact force per unit area is similar for components with the same aspect ratio. The quadratic regression curves fit the data well and those for the cylinders and disks are reproduced in Figures 16 and 17 where we compare the effect of sediment type on the rolling components and the effect of whether they are fixed or rolling on the coarser Dornach Firth sediment.

On the coarser sediment the drag of the fixed elements is greater than that of the rolling ones; the drag of the fixed cylinders is greater than the drag of the fixed disks; and the drag of the rolling cylinders and disks are very similar (Figure 16). On the finer sediment, however, the drag of the rolling cylinders is greater than that of the rolling disks (Figure 17). This figure

also demonstrates that the drag of the rolling components is greater on the finer sediment than it is on the coarser one.

4 Discussion

These trials provide a better understanding of the contact forces of towed demersal fishing gears and the seabed. They highlight that, to fully appreciate these forces, it is necessary to have a detailed knowledge of the weight and geometry of the gear components in contact with the sea bed, the sediment type and the nature of the contact (rolling or dragging).

On the coarser of the two sediments examined, the drag of the rectangular doors and (to a lesser extent) the fixed cylinders and disks reduces as towing speed increases (Figures 8 and 9). This effect appears to be more pronounced for the heavier components, but when the components roll on either sediment there is no apparent relationship between drag and towing speed (Figure 10).

This is the opposite of what we would normally expect. During soil deformation, there is an increase of the void space between sand particles which gives rise to a pressure gradient and drives an inflow of additional pore water from the surrounding soil. This is known as the common rate effect. In regions where the rate of the deformation is sufficiently high, the reductions of the pore pressure will be large and the voids will fill rapidly leading to an increase of the mean principle effective stress, an increase of the resistance of soil to shear and consequently an increase of the drag force required to deform the soil. At slower speeds, this effect is not so pronounced as there is more time for the pore water to fill the void space and the resulting pore pressure changes are small (Esmaeili and Ivanovic, 2014). During our trials, because our components are free to move in the vertical direction, it is possible that the

rate effect is offset by the gear components finding an equilibrium position that penetrates the seabed to a lesser depth when they are towed at higher speeds. Our results, however, are variable which may indicate that the interaction of the governing mechanisms is subtle and dependent on factors which can vary between and during tows such as seabed bathymetry (e.g. presence and size of sand ripples), sediment type and sea state and also on whether the components are fixed or are rolling.

The contact drag of the narrow disks and the cylinders are dependent on their aspect ratio when they are fixed on the coarser sediment and rolling on the finer sediment (Figures 16 and 17). For these cases the scaled drag of the very narrow disks (d/b = 8.0) is lower than that of the cylinders. This dependency is less apparent as the cylinders become wider (ie as d/b decreases), which suggests that for the wider cylinders soil failure is predominantly a two-dimensional phenomenon and that three dimensional effects such as pushing sediment sideways near the soil surface only play a role at the edges and hence, are only of particular importance for the narrow disks. On the coarser sediment there is no evidence of a dependence on the aspect ratio for the rolling cylinders and disks (Figure 17). The scaled contact drag of the very narrow disks and of the different cylinder categories is very similar. This suggests that when components roll on the coarser sediment the problem is two dimensional and there is unlikely to be any significant lateral displacement of sediment at the edges, where the geotechnical processes will be much the same as those of the central part of the wider cylinders.

The contact drag of the rolling cylinders is greater on the finer sediment than it is on the coarser one (Figure 17). This is likely to be due to greater penetration of these components into the sediment with larger clay and silt content and with a soft consistency.

While these results highlight the need to have a full understanding of the physical characteristics of the gear components, their dynamic constraints and the substrate on which they are towed, they are also significant in their own right as they can be used to identify simple design rules to aid the development of low impact demersal trawls. Research in this area has often focused on the use of lighter components and a reduction of the number of contact points with the seabed (Valdemarsen *et al*., 2007; He and Winger, 2010; Sterling and Eayrs, 2006; Rose *et al*., 2013; Fonteyne and Polet, 2002), but this has frequently been accompanied by a reduction in efficiency. For example a reduction of the weight of twin trawl clumps or modifications to the sweeps or groundgear can result in poorer contact of the fishing gear with the seabed and a subsequent loss of catch. Here we have shown, however that it is possible to keep the overall weight and contact area constant and significantly reduce contact drag by (i) using rolling components instead of fixed ones and (ii) using a number of narrow components instead of a single wide one. In particular we have demonstrated on the coarser sediment that the contact drag of rolling cylinders is less than half of what it is when they are fixed (Figure 16); and that on the finer sediment, the drag of six rolling separated disks is also less than half that when there are no spaces between them (Figure 17).

These data will also be very useful for testing and validating the numerical geotechnical models which are being developed to predict the contact forces and penetration into the seabed of individual gear components (Ivanović *et al*., 2011; Ivanović and O'Neill, 2015; Esmaeili and Ivanović, 2014) and in a number of other areas where similar processes occur such as: soil cutting and ploughing processes (Nouguier *et al*., 2000); iceberg interaction with the seabed (Yang and Poorooshasb, 1997; Barrette, 2011); vehicle mobility assessment (Bekker, 1969; Wong, 2001); and the indentation and rolling of wheels associated with off-road vehicles (Hambleton and Drescher, 2008, 2009). To characterize the geotechnical response of a wider range of sediment types, different constitutive stress/strain relationships

which underpin the numerical models are being explored and the accuracy and efficiency of the numerical methods are being investigated. These types of numerical models are likely to be one of the most productive ways forward. They will permit the quantitative assessment of the physical impact of towed demersal trawls and will contribute to the development of more fuel efficient gears; and in the longer term will form the basis of a more deterministic approach to assessing the broader ecological and environmental consequence of towing fishing gears in the benthic environment.

5 Acknowledgements

This study was funded in part by Fisheries Innovation Scotland, project FIS02, and by the FP7 project BENTHIS (312088). It does not necessarily reflect the views of the European Commission and does not anticipate the Commission's future policy in this area.

6 References

Barrette, P. 2011. Offshore pipeline protection against seabed gouging by ice: An overview, Cold Regions Science and Technology, 69: 3-20.

Bekker, M.G. 1969. Introduction to Terrain-Vehicle Systems, University of Michigan Press: Michigan.

Boulcott, P., Millar, C. P.,, and Fryer, R. J. 2014. Impact of scallop dredging on benthic epifauna in a mixed-substrate habitat. ICES Journal of Marine Science, 71: 834–844.

Brown, L., Bresnan, E., Summerbell K., and O'Neill F.G. 2013. The influence of demersal trawl fishing gears on the resuspension of dinoflagellate cysts. Marine Pollution Bulletin, 66, 17 – 24.

Depestele, J., Ivanović, A., Degrendele, K., Esmaeili, M., Polet, H., Roche, M., Summerbell, K., Teal, L.R., Vanelslander B., and O'Neill, F.G., 2016. Measuring and assessing the physical impact of beam trawling. ICES Journal of Marine Science. 73 (suppl 1): i15-i26.

Dounas, C., Davies, I., Triantafyllou, G., Koulouri, P., Petihakis, G., Arvanitidis, C., Sourlatzis, G., and Eleftheriou, A. 2007. Large-scale impacts of bottom trawling on shelf primary productivity. Cont. Shelf Res. 27, 2198–2210.

Drillet, G., Hay, S., Hansen, B. W., and O'Neill F.G. 2014. Effects of demersal otter trawls on the re-suspension of copepod resting eggs and its potential effects on recruitment. Journal of Fisheries and Livestock Production, 2:1. http://dx.doi.org/10.4172/2332-2608.1000114

Enerhaug, B., Ivanović, A., O'Neill, F.G., and Summerbell K. 2012. Friction Forces Between Seabed and Fishing Gear Components Proceedings of the 31th International

Conference on Ocean, Offshore and Arctic Engineering, OMAE 2012, Rio de Janeiro, Brazil, 1 – 6 July 2012.

Esmaeili, M., and Ivanović, A. 2014. Numerical Modeling of Fishing Ground Gear Component on the Seabed, Ocean Engineering, 91, 316–328.

FAO 2009. The state of world fisheries and aquaculture – 2008. Food and Agricultural Organisation of the United Nations, Rome. 176 pp.

Fonteyne, R., and Polet, H. 2002. Reducing the benthos by-catch in flatfish beam trawling by means of technical modifications. Fisheries Research, 55, 1–3, 219-230.

Gilkinson, K., Paulin, M., Hurley, S., and Schwinghamer, P. 1998. Impacts of trawl door scouring on infaunal bivalves: results of a physical trawl door model/dense sand interaction. Journal of Experimental Marine Biology and Ecology. Vol. 224, pp. 291-312.

Godwin, R.J., and O'Dogherty, M.J., 2007. Integrated soil tillage force prediction models. Journal of Terramechanics, 44, 3–14.

Hambleton, J.P., and Drescher, A., 2008. Modeling wheel-induced rutting in soils: Indentation. Journal of Terramechanics, 45:201-211.

Hambleton, J.P., and Drescher, A. 2009. Modeling wheel-induced rutting in soils: Rolling. Journal of Terramechanics, 46:34-47.

He, P., and Winger, P.D. 2010. Effect of trawling on the seabed and mitigation measures to reduce impact. Behaviour of marine fishes: capture processes and conservation challenges. Ed. P. He. Wiley-Blackwell, USA.

Humborstad, O.B., Nottestad, L., Løkkeborg, S., and Rapp, H.T. 2004. RoxAnn bottom classification system, sidescan sonar and video-sledge: spatial resolution and their use in assessing trawling impacts. ICES J. Mar. Sci. 61, 53-63.

Ivanović, A., Neilson, R.D., and O'Neill, F.G. 2011. Modelling the physical impact of trawl components on the seabed. Ocean Engineering, 38(7), 925-933.

Ivanović, A., and Casanovas Revilla, C., 2013. Analytical modeling of the resistance of the otter door. Proceedings of the 11th international workshop on methods for the development and evaluation of maritime technologies, Rostock 2013. Ed M. Paschen. Shaker Verlag, Aachen.

Ivanović, A., and O'Neill, F.G. 2015. Towing cylindrical fishing gear components on cohesive soils. Computers and Geotechnics. 65, 212 – 219.

Kaiser, M.J., Clarke, K.R., Hinz, H., Austen, M.C., Somerfield, P.I., and Karakassis, I. 2006. Global analysis of response and recovery of benthic biota to fishing. Marine Ecology Progress Series 311, 1-14.

Lucchetti, A., and Sala, A. 2012. Impact and performance of Mediterranean fishing gear by side-scan sonar technology. Can. J. Fish. Aquat. Sci. 69, 1806-1816.

Martín, J., Puig, P., Masque, P., Palanques, A., and, Sánchez-Gómez, A., 2014. Impact of Bottom Trawling on Deep-Sea Sediment Properties along the Flanks of a Submarine Canyon. PLoS ONE 9. PLoS ONE 9(8): e104536. doi:10.1371/journal.pone.0104536.

Nouguier, C., Bohatier, C., Morean, J.J., and, Radjai, F., 2000. Force fluctuations in a pushed granular material. Granular Matter, 2, 171–178.

Oberle, F.K.J, Swarzenski, P.W., Reddy, C.M., Nelson, R.K., Baasch, B., and Hanebuth T.J.J., 2016. Deciphering the lithological consequences of bottom trawling to sedimentary habitats on the shelf. Journal of Marine Systems. 159, 120 – 131.

O'Neill, F.G., Summerbell, K., and Breen, M. 2009. An underwater laser stripe seabed profiler to measure the physical impact of towed gear components on the seabed. Fish Res. 99:234-238.

O'Neill, F.G., and Summerbell, K. 2011. The mobilisation of sediment by demersal otter trawls. Mar. Pollut. Bull. 62, 1088-1097.

O'Neill F.G., Robertson, M., Summerbell K., Breen M., and Robinson, L.A. 2013. The mobilisation of sediment and benthic infauna by scallop dredges. Marine Environmental Research, 90, 104 – 112.

O'Neill, F.G. and Ivanović, A., 2016. The physical impact of towed demersal fishing gears on soft sediments. ICES Journal of Marine Science. 73 (suppl 1): i5-i14.

O'Neill, F.G., and Summerbell, K. 2016. The hydrodynamic drag and the mobilisation of sediment into the water column of towed fishing gear components. Journal of Marine Systems, 164, 76–84.

Palanques, A., Puig, P., Guillén, J., Demestre, M., and Martín, J. 2014. Effects of bottom trawling on the Ebro continental shelf sedimentary system (NW Mediterranean). Cont. Shelf Res. 72, 83-98.

Paschen, M., Richter, U., and, Köpnick, W. 2002. Trawl penetration in The Seabed (TRAPESE), EC-Final Report, Contract No. 96-006, Univ. of Rostock.

Puig, P., Canals, M., Company, J., Martin, J., Amblas, D., Lastras, G., Palanques, A., and Calafat, A.M. 2012. Ploughing the deep sea floor. Nature 489, 286-289.

Rose, C.S., Hammond, C.F., Stoner, A.W., Munk, J.E., and Gauvin. J.R. 2013. Quantification and reduction of unobserved mortality rates for snow, southern Tanner, and red king crabs (Chionoecetes opilio, C. bairdi, and Paralithodes camtschaticus) after encounters with trawls on the seafloor, Fishery Bulletin, 111; 42–53.

Sterling, D., and Eayrs, S. 2006. Design and assessment of two gear modifications to reduce the benthic impact and fuel intensity of prawn trawling in Australia. Presented at the ICES Symposium on Fishing Technology in the 21rst Century. Boston, MA, USA.

Valdemarsen J., Jorgesen T., and Engas A. 2007. Options to mitigate bottom habitat impact. FAO Fisheries Technical Paper, No T506. Food and Agriculture Oranisation of the United Nations, Rome, pp.1-29.

Wong J.Y. 2001. Theory of Ground vehicle, Wiley: New York.

Yang Q.S., and Poorooshasb H.B. 1997. Numerical modeling of seabed ice scour. Computers and Geotechnics, 21: 1-20.

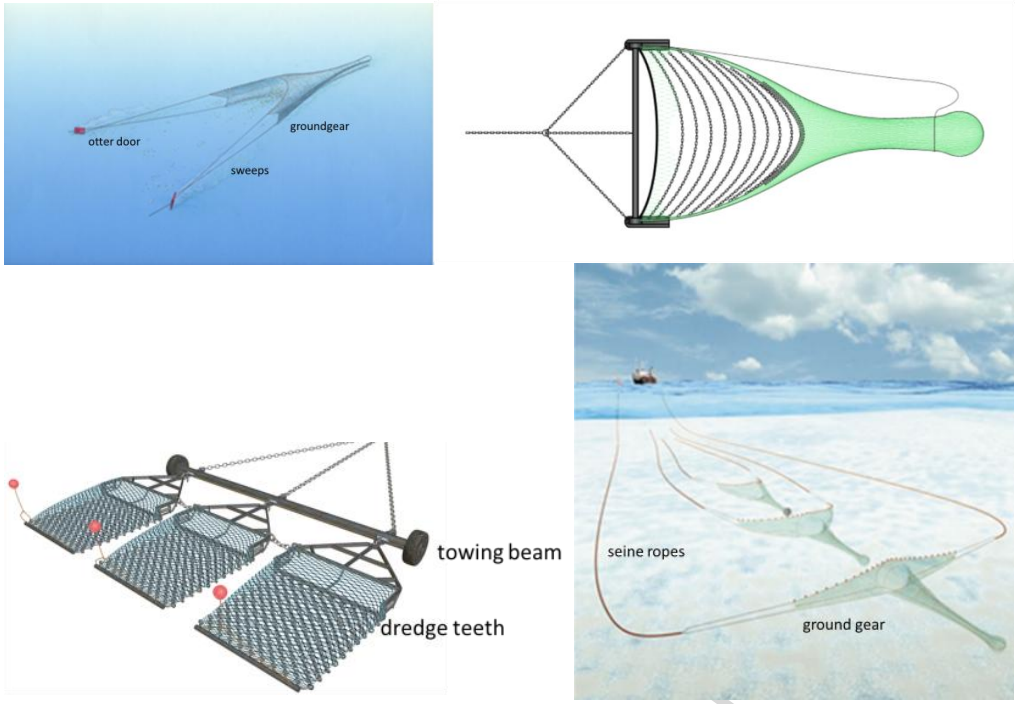

Figure 1. Examples of towed demersal fishing gears. (Going clockwise) A demersal otter trawl, a tickler chain beam trawl, three scallop dredges on a single beam and a demersal seine net with some of the components that are in contact with the seabed identified.

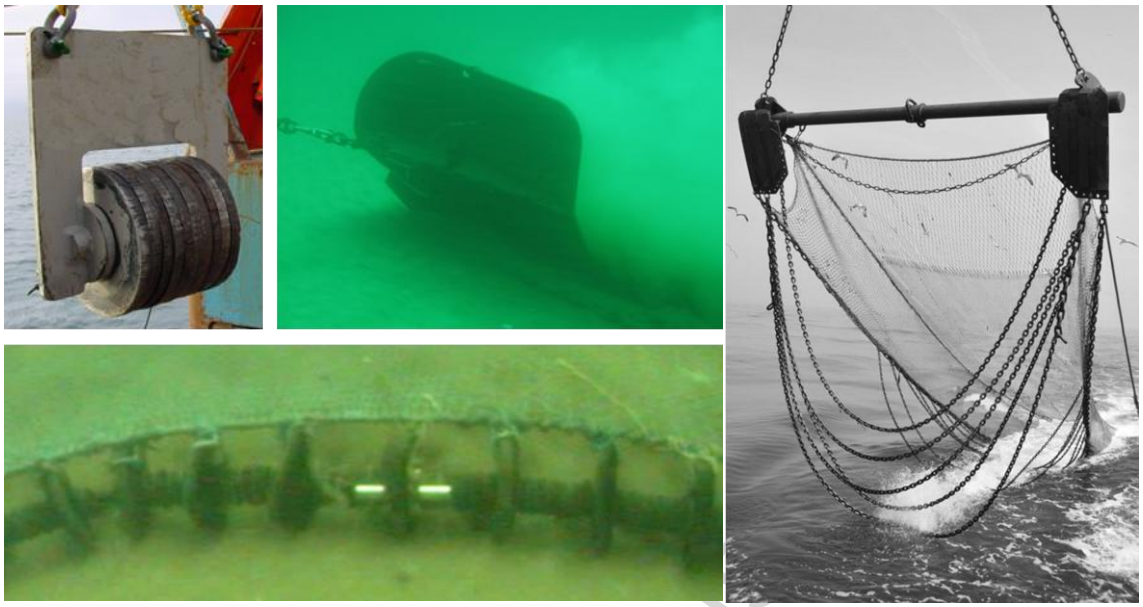

Figure 2. Some components of towed demersal fishing gears: (In the clockwise direction) a roller clump which is used in twin trawls to maintain contact with the seabed; otter doors which spread the gear; the shoes and ticker chains of a beam trawl and a rockhopper groundgear which maintains contact with and protect the netting from the seabed.

Figure 3 The towed sledge, sitting upright, used to tow the range of cylindrical objects supported on an axle.

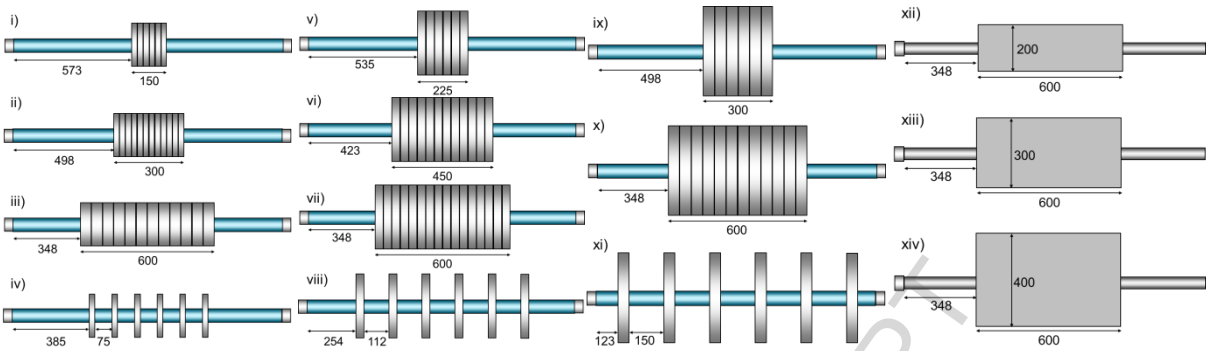

Figure 4. The range of gear components designed to simulate some of the groundgears, clump weights and doors used in demersal fisheries comprising disks, cylinders and trawl doors. All measurements are in millimetres.

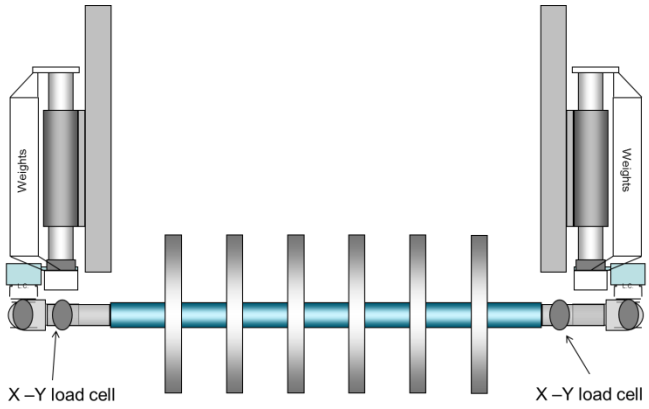

Figure 5. The framework to which the gear components and axle were attached showing where the additional weights were fitted and the position of the two Strainstall 500kg X-Y load cells.

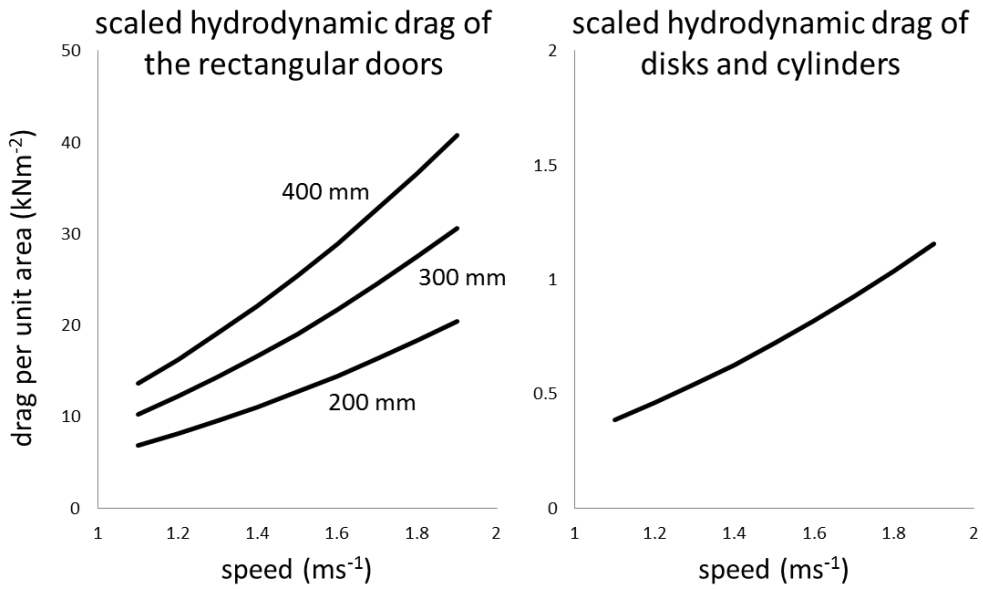

Figure 6. The scaled hydrodynamic drag estimates of the gear components. The area scale of the disks and cylinders is equal to A_{elem} hence their scaled hydrodynamic drag can be represented by one curve.

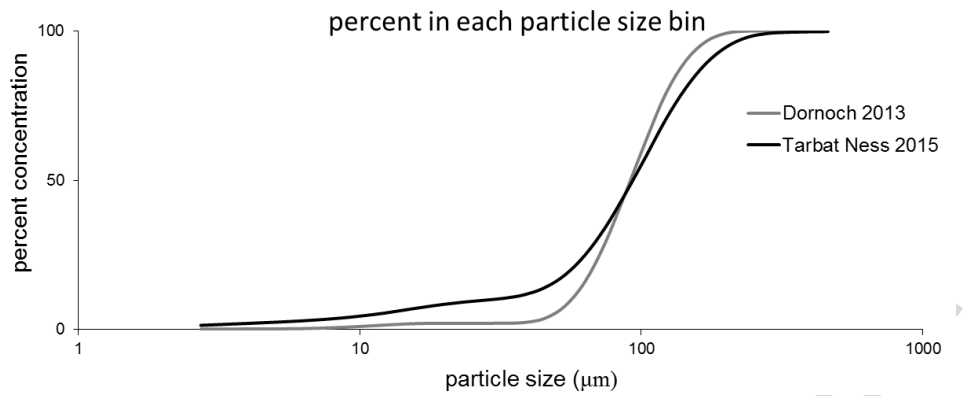

Figure 7. The particle size distribution of the sediment at each site. At the Dornoch Firth site in 2013 the silt and clay component was 12% and the d50 was 100 μm. At the site east north east of Tarbat Ness in 2015 the sediment was finer and the silt and clay component was 30% and the d50 was 85 μm.

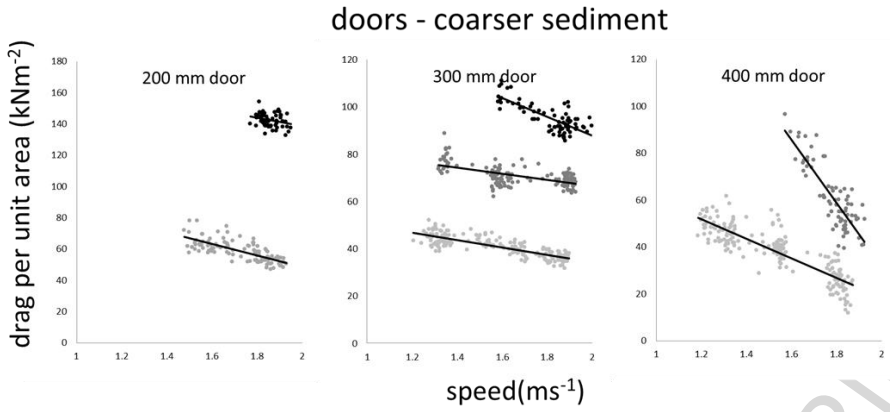

Figure 8 The contact drag measurements (and their linear regressions) for the rectangular doors plotted against towing speed from the 2013 trials on the coarser Dornach Firth sediment. The light grey, dark grey and black points are the data when the vertical forces (in water) were approximately 588, 1176 and 1764 N respectively. (Note, the *y* axis scale varies between plots)

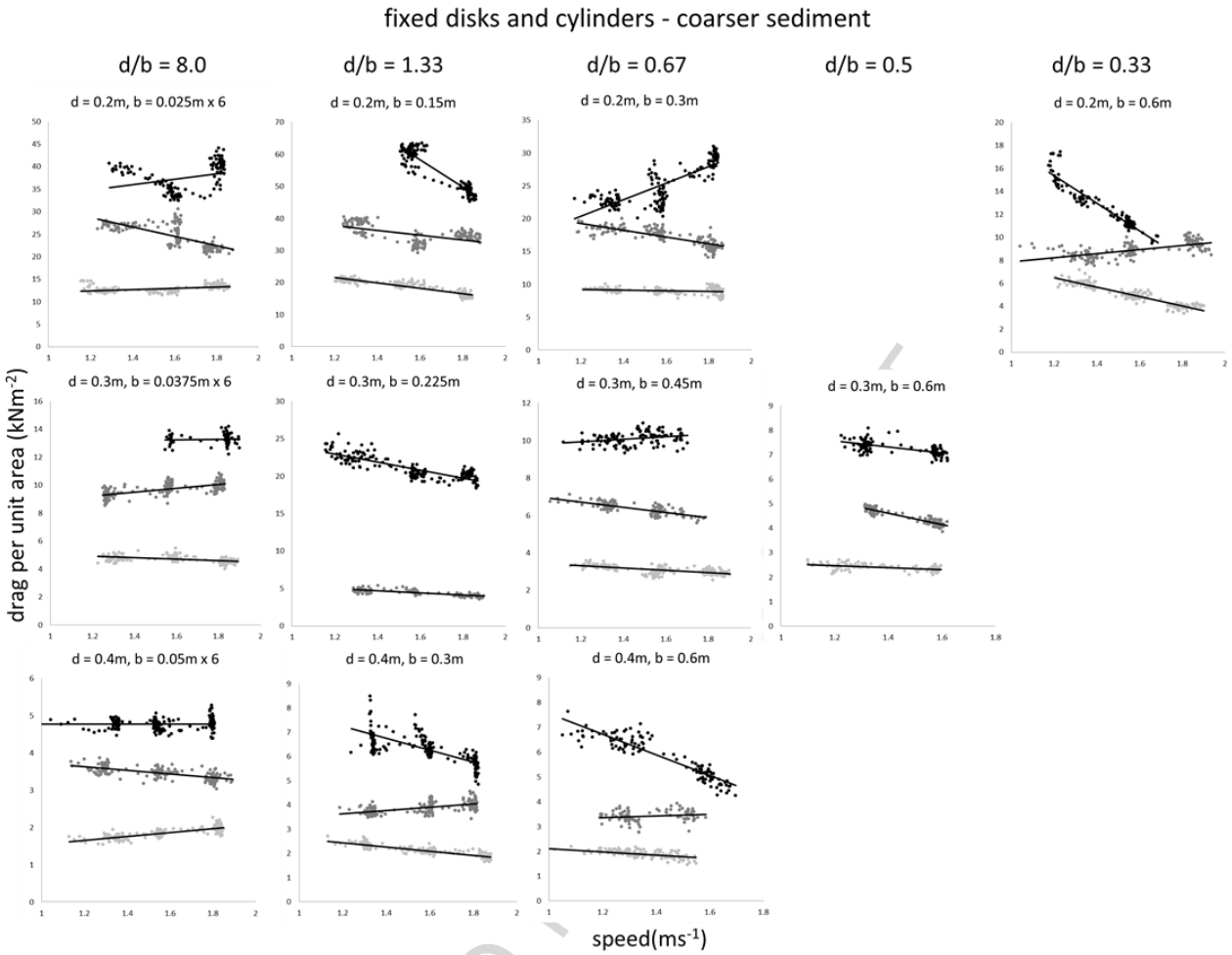

Figure 9 The contact drag measurements (and their linear regressions) for the fixed circular disks and cylindrical components plotted against towing speed from the 2013 trials on the coarser Dornach Firth sediment. The light grey, dark grey and black points are the data when the vertical forces (in water) were approximately 588, 1176 and 1764 N respectively. (Note, the *x* and *y* axis scales vary between plots)

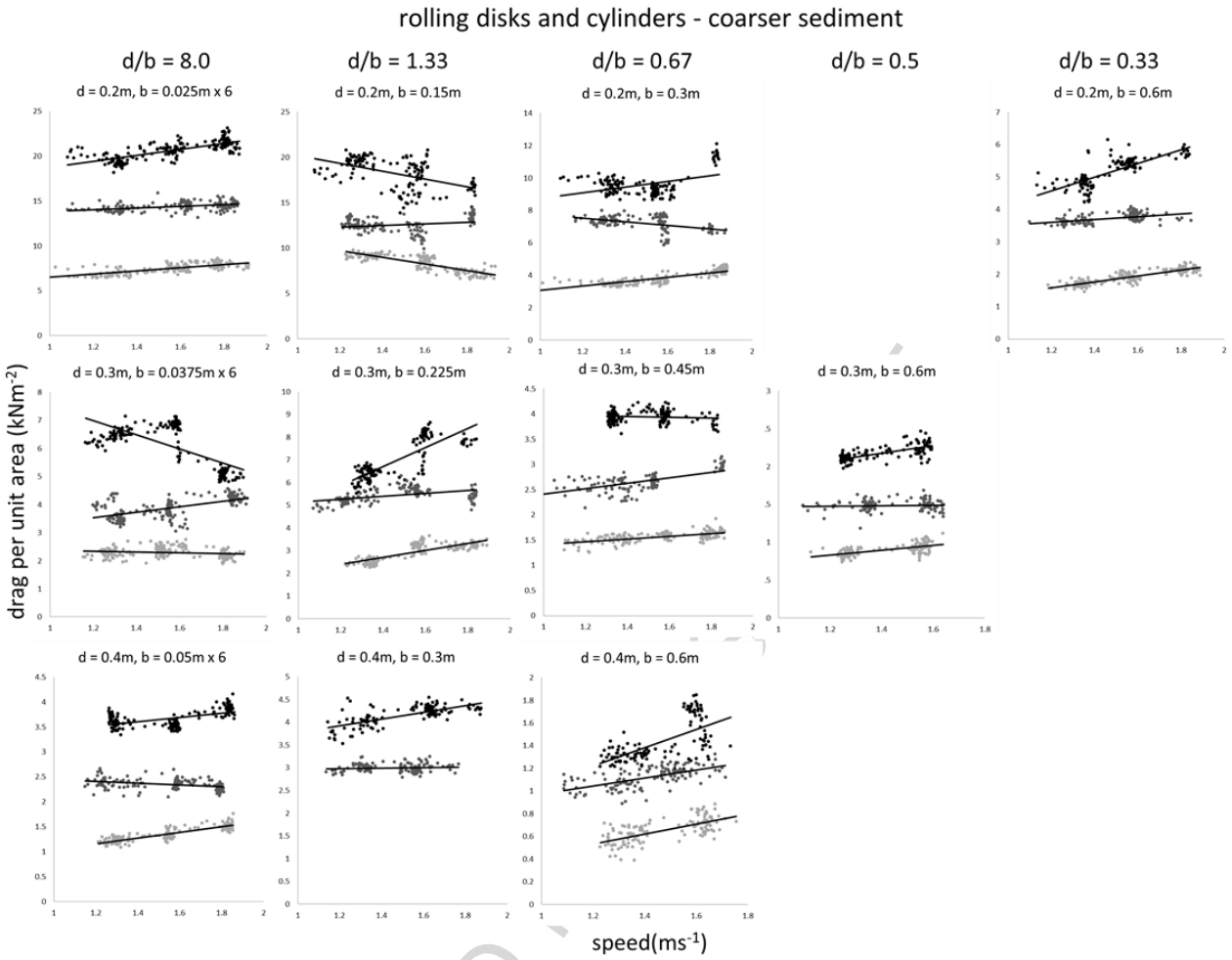

Figure 10 The contact drag measurements (and their linear regressions) for the rolling circular disks and cylindrical components plotted against towing speed from the 2013 trials on the coarser Dornach Firth sediment. The light grey, dark grey and black points are the data when the vertical forces (in water) were approximately 588, 1176 and 1764 N respectively. (Note, the *x* and *y* axis scales vary between plots)

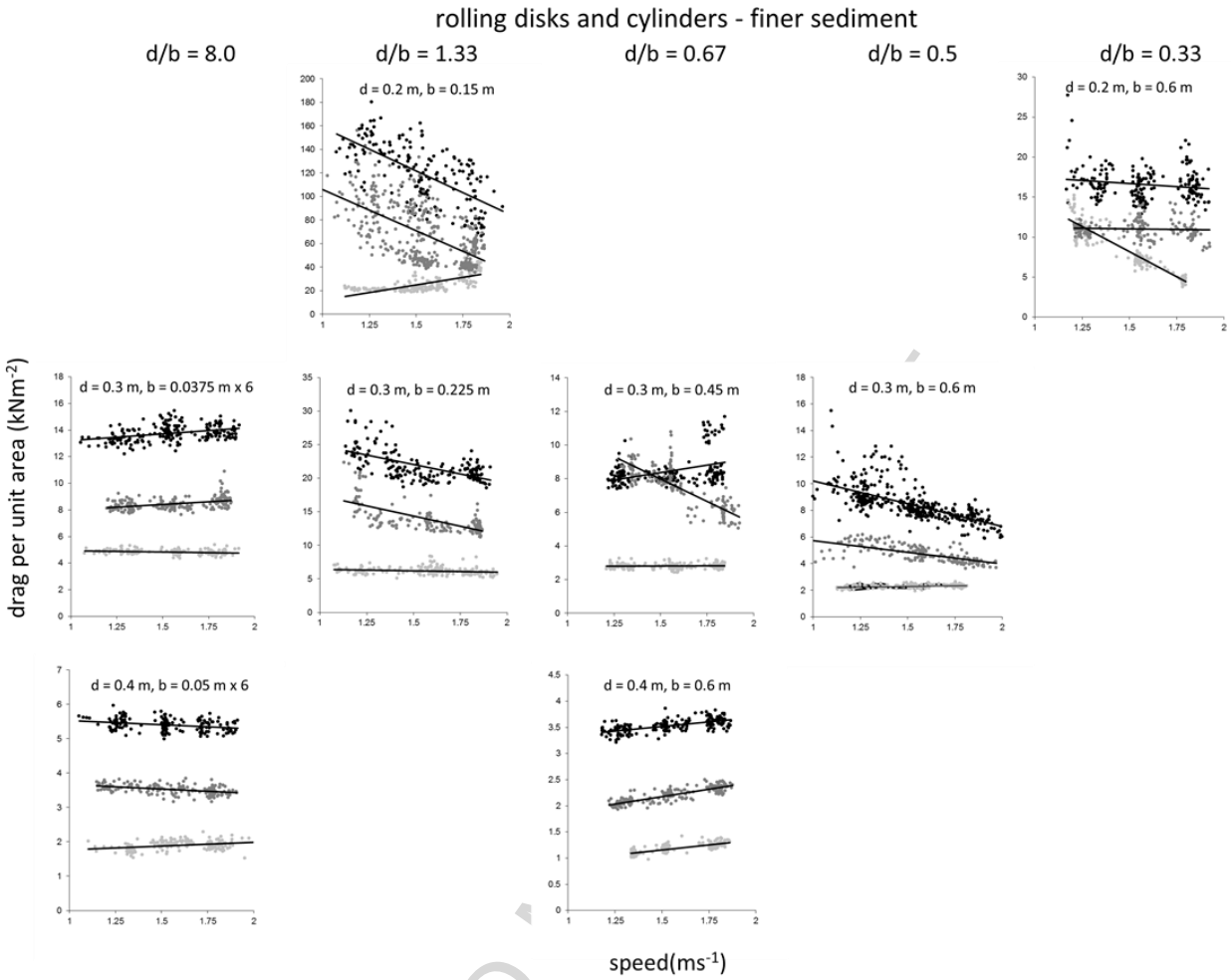

Figure 11 The contact drag measurements (and their linear regressions) for the rolling circular disks and cylindrical components plotted against towing speed from the 2015 trials on the finer sediment east north east of Tarbat Ness. The light grey, dark grey and black points are the data when the vertical forces (in water) were approximately 588, 1176 and 1764 N respectively. (Note, the *y* axis scale varies between plots)

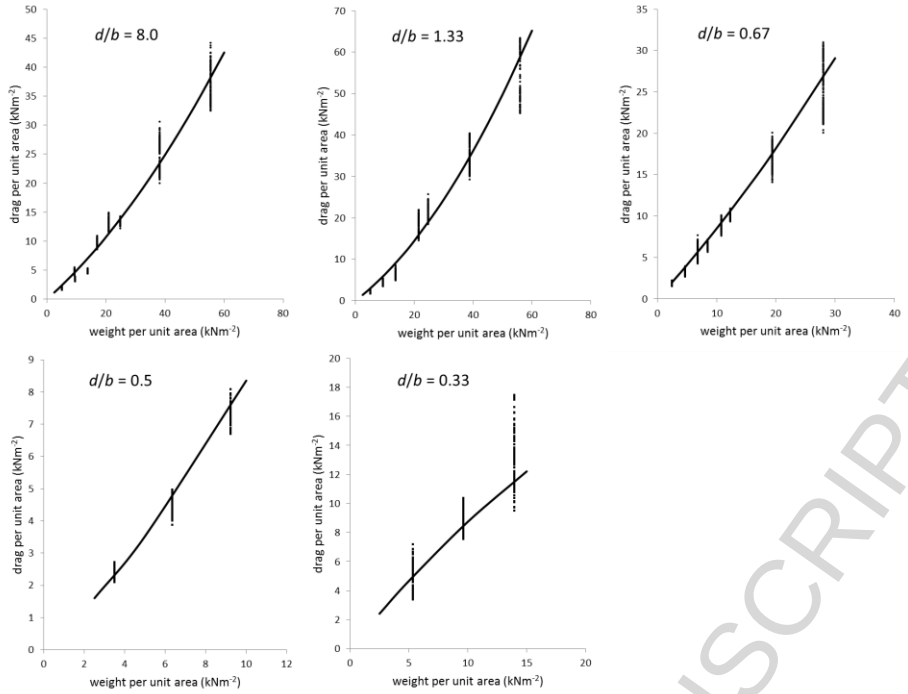

Figure 12 The contact drag measurements for the fixed circular disks and cylindrical components plotted against weight per unit area from the 2013 trials on the coarser Dornach Firth sediment where each plot represents a different aspect ratio group (Note, the *x* and *y* axis scales vary between plots). The curves are quadratic regression with a zero intercept.

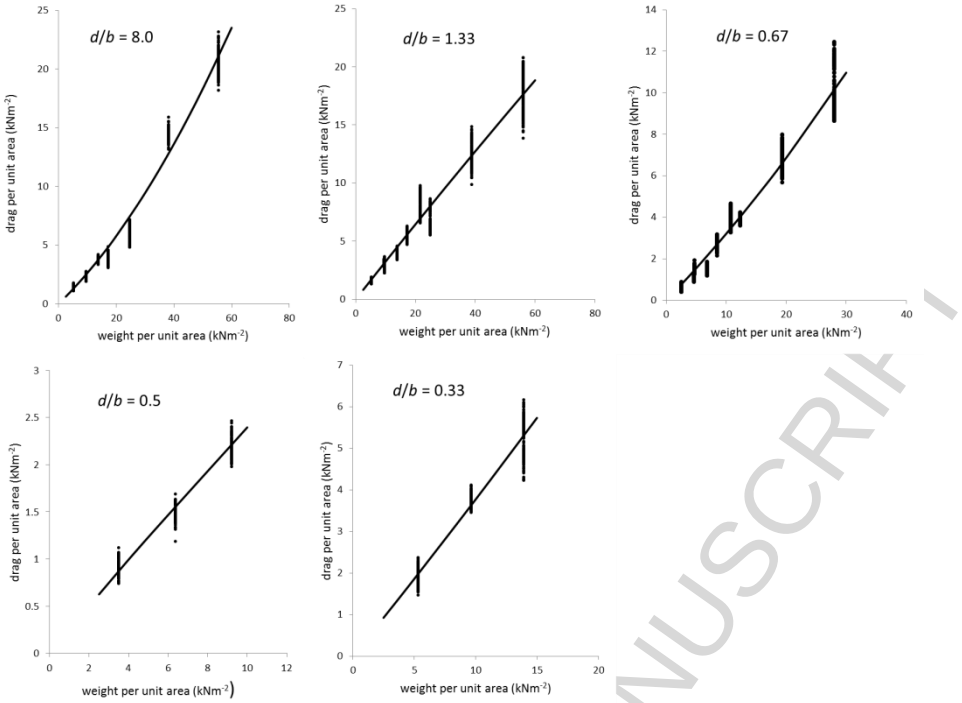

Figure 13 The contact drag measurements for the rolling circular disks and cylindrical components plotted against weight per unit area from the 2013 trials on the coarser Dornach Firth sediment where each plot represents a different aspect ratio group (Note, the *x* and *y* axis scales vary between plots). The curves are quadratic regression with a zero intercept.

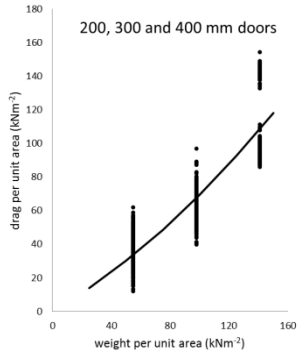

Figure 14 The contact drag measurements for the rectangular doors plotted against weight per unit area from the 2013 trials on the coarser Dornach Firth sediment.

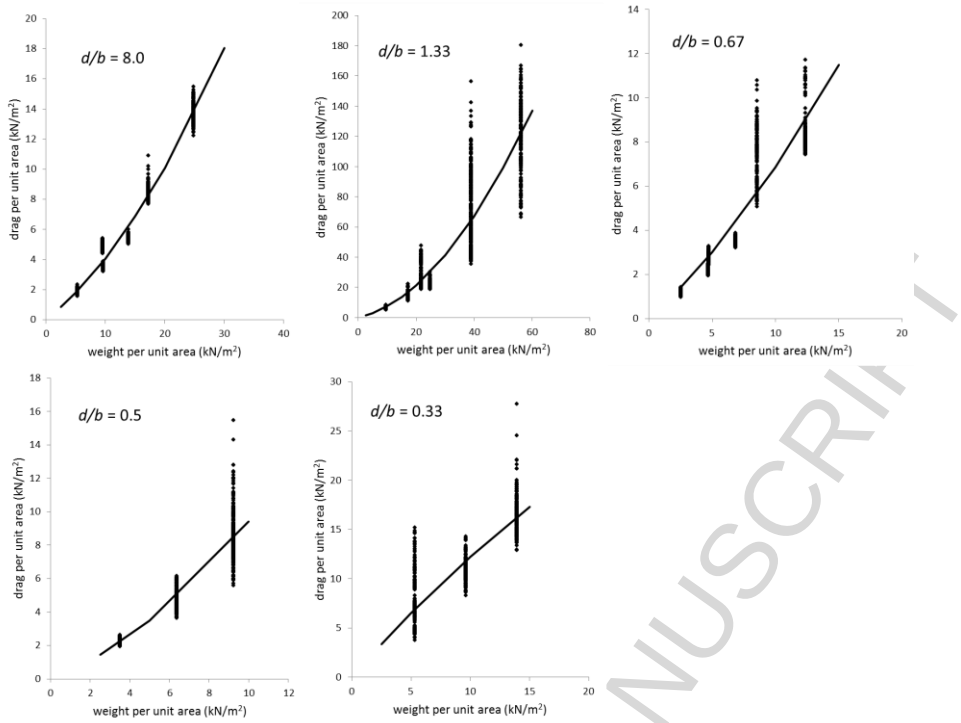

Figure 15. The contact drag measurements for the rolling circular disks and cylindrical components plotted against towing speed from the 2015 trials on the finer sediment east north east of Tarbat Ness where each plot represents a different aspect ratio group (Note, the *x* and *y* axis scales vary between plots).

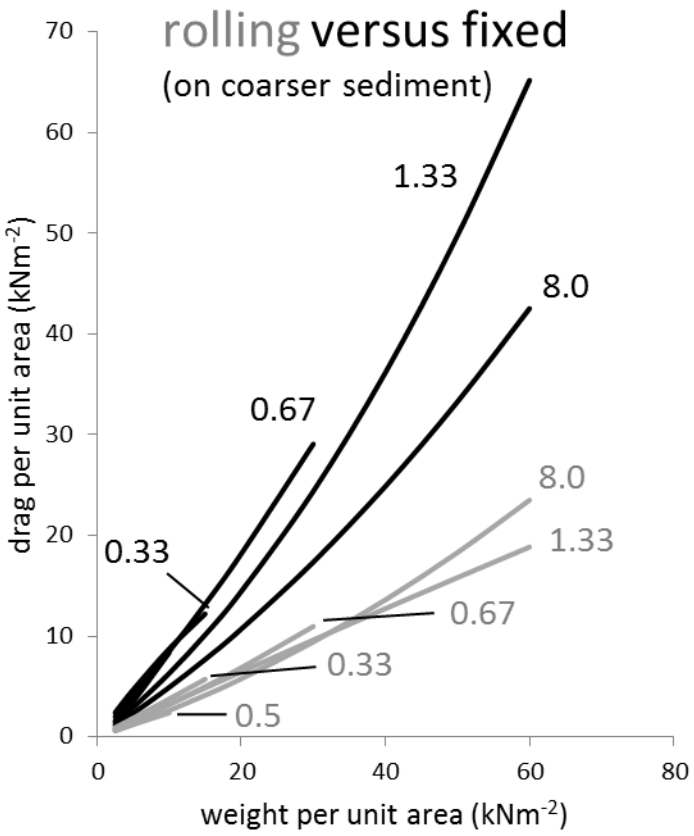

Figure 16. Comparison of the fixed and rolling cylinders on the coarser Dornach Firth sediment. The black lines are the fitted curves of figure 11 for the fixed cylinders and disks. The grey lines are the fitted curves of figure 12 for the rolling cylinders and disks. The labels are the aspect ratio group that each curve represents. (The 0.5 curve for the fixed cylinders and disks cannot be distinguished from the 0.33 curve in this plot).

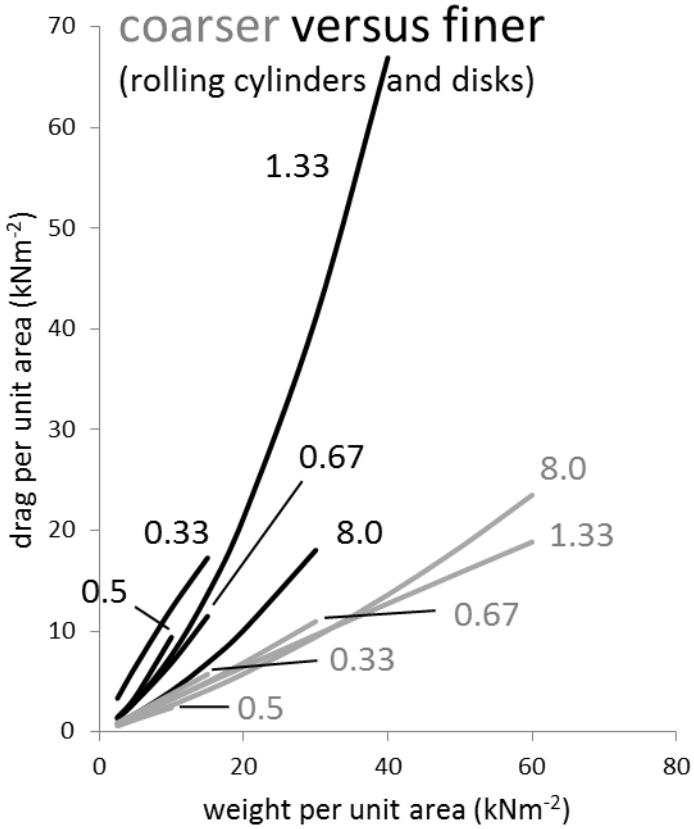

Figure 17 Comparison of the rolling cylinders and disks on the coarser and finer sediments. The grey lines are the fitted curves of figure 12 for the rolling cylinders and disks on the coarser Dornach Firth sediment. The black lines are the fitted curves of figure 14 for the rolling cylinders and disks on the finer sediment east north east of Tarbat Ness. The labels are the aspect ratio group that each curve represents.

Table 1. The dimensions and diameter to breadth ratio of the components tested during the experimental sea trials. The labels correspond to the diagrams of figure 4.

	cylinders				
labels	*d* (diameter)	*b* (breadth)	A_{elem} *(= bd)*	*d/b*	Godwin & O'Dogherty (2007)
i	0.2	0.15	0.03	1.33	narrow
ii	0.2	0.3	0.06	0.67	intermediate
iii	0.2	0.6	0.12	0.33	wide
v	0.3	0.225	0.0675	1.33	narrow
vi	0.3	0.45	0.135	0.67	intermediate
vii	0.3	0.6	0.18	0.5	intermediate
ix	0.4	0.3	0.12	1.33	narrow
x	0.4	0.6	0.24	0.67	intermediate
	disks				
	d (diameter)	*b* (breadth)	A_{elem} *(= 6bd)*	*d/b*	Godwin & O'Dogherty (2007)
iv	0.2	0.025	0.03	8	very narrow
viii	0.3	0.0375	0.0675	8	very narrow
xi	0.4	0.05	0.12	8	very narrow
	rectangular doors				
	h (height)	*b* (breadth)	A_{elem} *(= hb)*	*h/b*	*t* (thickness)
xii	0.2	0.6	0.12	0.33	0.02
xiii	0.3	0.6	0.18	0.5	0.02
xiv	0.4	0.6	0.24	0.67	0.02